

Low-Latency Tracking of Multiple Permanent Magnets

Cameron R. Taylor, Haley G. Abramson, and Hugh M. Herr

Abstract—Magnetic target tracking is a low-cost, portable, and passive method for tracking materials wherein magnets are physically attached or embedded without the need for line of sight. Traditional magnet tracking techniques use optimization algorithms to determine the positions and orientations of permanent magnets from magnetic field measurements. However, such techniques are constrained by high latencies, primarily due to the numerical calculation of the gradient. In this study, we derive the analytic gradient for multiple-magnet tracking and show a dramatic reduction in tracking latency. We design a physical system comprising an array of magnetometers and one or more spherical magnets. To validate the performance of our tracking algorithm, we compare the magnet tracking estimates with state-of-the-art motion capture measurements for each of four distinct magnet sizes. We find comparable position and orientation errors to state-of-the-art magnet tracking, but demonstrate increased maximum bandwidths of 336%, 525%, 635%, and 773% for the simultaneous tracking of 1, 2, 3, and 4 magnets, respectively. We further show that it is possible to extend the analytic gradient to account for disturbance fields, and we demonstrate the simultaneous tracking of 1 to 4 magnets with disturbance compensation. These findings extend the use of magnetic target tracking to high-speed, real-time applications requiring the tracking of one or more targets without the constraint of a fixed magnetometer array. This advancement enables applications such as low-latency augmented and virtual reality interaction, volitional or reflexive control of prostheses and exoskeletons, and simplified multi-degree-of-freedom magnetic levitation.

Index Terms—Magnetic dipole tracking, position and orientation tracking, permanent magnets, analytic Jacobian, disturbance field compensation, magnetic anomaly detection, passive wireless device tracking, magnetization, sensors, human-computer interfaces, virtual reality, augmented reality

I. INTRODUCTION

MAGNETS have been used to track fingers [1], [2], styli [3], jewelry [4], vibrating beams [5], endoscopes [6], [7], catheters [8], tongues [9], jaws [10], bladders [11], heart valves [12], and joints [13]–[15], and have also been suggested for tracking other biological tissue such as muscle [16]. As demonstrated by this extensive formative work on magnet tracking, using permanent magnets as position markers is advantageous because there is no need to power them via wired or wireless power transmission. In addition, many materials, such as wood, plastic, ceramic, rubber, and human flesh (materials with magnetic permeability close to that of free space) allow magnetic fields to pass through them undisturbed, so magnets can be tracked through each material as if the material was not present.

Manuscript received Month xx, 2xxx; revised Month xx, xxxx; accepted Month x, xxxx. This work was supported by the MIT Media Lab Consortium.

The authors are with the MIT Center for Extreme Bionics, Massachusetts Institute of Technology, Cambridge, MA 02142, USA (email: hherr@media.mit.edu).

The magnetic dipole model is widely used throughout the literature to track permanent magnets. This model most accurately characterizes the field around a uniformly magnetized spherical object [17], but using the far field of magnetized objects, the dipole model has also been used to track and characterize nonspherical permanent magnets, electromagnets [18], and ferromagnetic objects such as cars [19], spacecraft [20], underwater magnetic anomalies [21], and mineral deposits [22].

A primary challenge in magnet tracking, however, is that determining magnet states (i.e., locations, orientations, and strengths) from an array of magnetic field sensors is not guaranteed to have a closed form solution. Thus, the state of a magnet is commonly determined using optimization techniques [23] or neural networks [24], which for an increased number of degrees of freedom historically suffer from large latency or convergence to local minima [25].

Further, accurate magnet tracking also requires compensation for disturbance fields, which is typically done as a one-time offset for static scenarios or via an external device such as an additional sensor [26] or magnetic shield [27]. Though the utility of these methods should not be understated, they nonetheless present a challenge in some mobile contexts. Recent foundational work has shown the ability to compensate for disturbance fields using a magnetometer array [28], but this compensation introduces additional delay to latencies already unsuitable for high-bandwidth tracking of multiple magnets.

We present here an algorithm for tracking any number of magnets of any size simultaneously with high accuracy and low computational latency, while compensating for disturbance fields in real time. We achieve these results via an analytic solution to the derivative (i.e., the Jacobian matrix) of the magnet tracking cost function with respect to each of the magnet state parameters. Whereas a traditional magnet tracking optimization must compute cost function data in each dimension to numerically perform gradient descent, the analytic Jacobian matrix provides a rapid, high-accuracy representation of the gradient, and thus significantly reduces tracking delay.

While the use of an analytic Jacobian matrix has been demonstrated previously for offline localization of multiple static axisymmetric magnets [29], we specifically focus on the tracking of spherical magnets with the dipole model in order to optimize the speed of evaluation for real-time tracking. To validate the performance of our tracking algorithm, we design a physical system comprising an array of magnetometers and one or more spherical magnets (diameters 2, 4, 8, and 16 mm). For these magnets, we compare the state estimates from this tracking algorithm against state-of-the-art motion capture measurements.

II. MATERIALS AND METHODS

A. Tracking Algorithm

A commonly used method of tracking permanent magnets utilizes an optimization algorithm. At each step of the optimization, each of the magnet parameters (locations, orientations, and/or strengths) is estimated. Note that magnet strengths need not be estimated once they are known, but estimating the magnet strengths using the tracking algorithm can correct for errors in the factory specifications of magnets as well as their relationship to sensor gains. The estimate of magnet parameters is used to calculate a predicted magnetic field at each known sensor location in a sensor array. Comparing the magnetic field prediction with the actual magnetic field measurement at each sensor, a magnetic field prediction error is then computed corresponding to the current estimate of the magnet parameters. In the case of a gradient descent optimization, the derivative of the prediction error (i.e., the Jacobian matrix of the prediction error) is then determined with respect to each of the magnet parameter estimates, and these derivatives are used to update the magnet parameter estimates until the prediction error is minimized. The magnet parameters determined from the optimization solution are then used as the initial estimate to the subsequent tracking step.

The derivatives of the magnetic field prediction error are typically computed numerically. Computing these derivatives numerically is time intensive because it requires the prediction error to be computed at least once for every magnet parameter being tracked. The added computational time places limitations on real-time tracking bandwidth and, when the tracked magnets change position rapidly, can result in tracking instability.

We describe below a tracking algorithm, implementing the use of analytic derivatives, to track spherical magnets via an optimization algorithm. The analytic derivatives in this tracking algorithm are implemented in a manner that has the benefits of numerical stability and allows for a significant decrease in latency compared with the latency inherent to other algorithms. Further, this tracking method is extended to the tracking of disturbance fields.

1) *Cost Function:* We will use the magnetic field prediction error for our optimization cost function. At the i th sensor, the magnetic field prediction error, \mathbf{E}_i , is the difference between the measured magnetic field $\tilde{\mathbf{B}}_i$ and the predicted magnetic field \mathbf{B}_i ,

$$\mathbf{E}_i = \mathbf{B}_i - \tilde{\mathbf{B}}_i. \quad (1)$$

To compute the predicted magnetic field \mathbf{B}_i , we use our estimate of the magnet locations, orientations, and strengths.

If the estimated location of the j th magnet is (x_j, y_j, z_j) and the position of the i th sensor is (s_{ix}, s_{iy}, s_{iz}) , it follows that a vector from the j th magnet to the i th sensor is given by

$$\mathbf{r}_{ij} = (s_{ix} - x_j)\hat{\mathbf{x}} + (s_{iy} - y_j)\hat{\mathbf{y}} + (s_{iz} - z_j)\hat{\mathbf{z}}, \quad (2)$$

where, for simplicity, we will define \bar{x}_{ij} , \bar{y}_{ij} and \bar{z}_{ij} such that

$$\mathbf{r}_{ij} = \bar{x}_{ij}\hat{\mathbf{x}} + \bar{y}_{ij}\hat{\mathbf{y}} + \bar{z}_{ij}\hat{\mathbf{z}}. \quad (3)$$

Using the positive z -axis as an arbitrarily-chosen reference, the orientation of the j th magnet can be described by

$$\begin{aligned} \mathbf{m}_j &= \mathbf{R}_z(\phi_j)\mathbf{R}_y(\theta_j)m_j\hat{\mathbf{z}} \\ &= m_j(\sin\theta_j \cos\phi_j\hat{\mathbf{x}} + \sin\theta_j \sin\phi_j\hat{\mathbf{y}} + \cos\theta_j\hat{\mathbf{z}}), \end{aligned} \quad (4)$$

where θ_j and ϕ_j are the magnet's estimated orientation from vertical and around vertical, respectively, and m_j is the magnet's strength, or magnetic moment. By the definition of the magnetic moment, we have

$$m_j = \frac{B_{rj}}{\mu_0} \frac{4}{3} \pi R_j^3, \quad (5)$$

where B_{rj} is the j th magnet's residual flux density, R_j is its radius, and μ_0 is the permeability of free space. If we define the magnetic dipole weight of the j th magnet as

$$\bar{\mathbf{m}}_j = \frac{\mu_0}{4\pi} \mathbf{m}_j, \quad (6)$$

the strength of the magnet can be expressed more simply as

$$\bar{m}_j = \frac{B_{rj}}{3} R_j^3. \quad (7)$$

Using the equation for the magnetic field of a dipole [17], the magnetic field prediction $\mathbf{B}_i = (B_{ix}, B_{iy}, B_{iz})$ at the i th sensor can then be expressed as

$$\mathbf{B}_i = \mathbf{G} + \sum_{j'=1}^{j'=M} \left(\frac{3\mathbf{r}_{ij'}(\bar{\mathbf{m}}_{j'}^T \cdot \mathbf{r}_{ij'})}{r_{ij'}^5} - \frac{\bar{\mathbf{m}}_{j'}}{r_{ij'}^3} \right), \quad (8)$$

where $\mathbf{G} = (G_x, G_y, G_z)$ is an estimate of the spatially uniform disturbance field and M is the number of magnets.

Substituting (6), (4) and (3) into (8), the three components of \mathbf{B}_i are given by (8a), (8b), and (8c) below.

$$B_{ix} = G_x + \sum_{j'=1}^{j'=M} \bar{m}_{j'} \left(\frac{3\bar{x}_{ij'}(\sin\theta_{j'} \cos\phi_{j'}\bar{x}_{ij'} + \sin\theta_{j'} \sin\phi_{j'}\bar{y}_{ij'} + \cos\theta_{j'}\bar{z}_{ij'})}{(\bar{x}_{ij'}^2 + \bar{y}_{ij'}^2 + \bar{z}_{ij'}^2)^{5/2}} - \frac{\sin\theta_{j'} \cos\phi_{j'}}{(\bar{x}_{ij'}^2 + \bar{y}_{ij'}^2 + \bar{z}_{ij'}^2)^{3/2}} \right) \quad (8a)$$

$$B_{iy} = G_y + \sum_{j'=1}^{j'=M} \bar{m}_{j'} \left(\frac{3\bar{y}_{ij'}(\sin\theta_{j'} \cos\phi_{j'}\bar{x}_{ij'} + \sin\theta_{j'} \sin\phi_{j'}\bar{y}_{ij'} + \cos\theta_{j'}\bar{z}_{ij'})}{(\bar{x}_{ij'}^2 + \bar{y}_{ij'}^2 + \bar{z}_{ij'}^2)^{5/2}} - \frac{\sin\theta_{j'} \sin\phi_{j'}}{(\bar{x}_{ij'}^2 + \bar{y}_{ij'}^2 + \bar{z}_{ij'}^2)^{3/2}} \right) \quad (8b)$$

$$B_{iz} = G_z + \sum_{j'=1}^{j'=M} \bar{m}_{j'} \left(\frac{3\bar{z}_{ij'}(\sin\theta_{j'} \cos\phi_{j'}\bar{x}_{ij'} + \sin\theta_{j'} \sin\phi_{j'}\bar{y}_{ij'} + \cos\theta_{j'}\bar{z}_{ij'})}{(\bar{x}_{ij'}^2 + \bar{y}_{ij'}^2 + \bar{z}_{ij'}^2)^{5/2}} - \frac{\cos\theta_{j'}}{(\bar{x}_{ij'}^2 + \bar{y}_{ij'}^2 + \bar{z}_{ij'}^2)^{3/2}} \right) \quad (8c)$$

2) *Analytic Jacobian*: Having fully developed the cost function (1) for our optimization, we now seek to form the Jacobian matrix, a matrix of the derivatives of the cost function elements with respect to each of the estimated magnet parameters ($x_j, y_j, z_j, \theta_j, \phi_j$ and \bar{m}_j) for each of the magnets.

We know that the measured magnetic field $\tilde{\mathbf{B}}_i$ does not vary with respect to our estimated magnet parameters (for example, $\partial/\partial x_j \mathbf{E}_i = \partial/\partial x_j \mathbf{B}_i$), so the derivatives of the cost function can be written as a function of \mathbf{B}_i alone. Thus, the Jacobian submatrix corresponding to the i th sensor and j th magnet can be calculated as

$$\mathbf{J}_{ij} = \begin{bmatrix} \frac{\partial}{\partial x_j} E_{ix} & \frac{\partial}{\partial y_j} E_{ix} & \frac{\partial}{\partial z_j} E_{ix} & \frac{\partial}{\partial \theta_j} E_{ix} & \frac{\partial}{\partial \phi_j} E_{ix} & \frac{\partial}{\partial \bar{m}_j} E_{ix} \\ \frac{\partial}{\partial x_j} E_{iy} & \frac{\partial}{\partial y_j} E_{iy} & \frac{\partial}{\partial z_j} E_{iy} & \frac{\partial}{\partial \theta_j} E_{iy} & \frac{\partial}{\partial \phi_j} E_{iy} & \frac{\partial}{\partial \bar{m}_j} E_{iy} \\ \frac{\partial}{\partial x_j} E_{iz} & \frac{\partial}{\partial y_j} E_{iz} & \frac{\partial}{\partial z_j} E_{iz} & \frac{\partial}{\partial \theta_j} E_{iz} & \frac{\partial}{\partial \phi_j} E_{iz} & \frac{\partial}{\partial \bar{m}_j} E_{iz} \end{bmatrix} = \begin{bmatrix} \frac{\partial}{\partial x_j} B_{ix} & \frac{\partial}{\partial y_j} B_{ix} & \frac{\partial}{\partial z_j} B_{ix} & \frac{\partial}{\partial \theta_j} B_{ix} & \frac{\partial}{\partial \phi_j} B_{ix} & \frac{\partial}{\partial \bar{m}_j} B_{ix} \\ \frac{\partial}{\partial x_j} B_{iy} & \frac{\partial}{\partial y_j} B_{iy} & \frac{\partial}{\partial z_j} B_{iy} & \frac{\partial}{\partial \theta_j} B_{iy} & \frac{\partial}{\partial \phi_j} B_{iy} & \frac{\partial}{\partial \bar{m}_j} B_{iy} \\ \frac{\partial}{\partial x_j} B_{iz} & \frac{\partial}{\partial y_j} B_{iz} & \frac{\partial}{\partial z_j} B_{iz} & \frac{\partial}{\partial \theta_j} B_{iz} & \frac{\partial}{\partial \phi_j} B_{iz} & \frac{\partial}{\partial \bar{m}_j} B_{iz} \end{bmatrix}. \quad (9)$$

The first three columns of derivatives in (9) are written in terms of x_j, y_j , or z_j , but \mathbf{B}_i in (8a), (8b), and (8c) is written in terms of \bar{x}_j, \bar{y}_j , and \bar{z}_j . From the definitions of \bar{x}_j, \bar{y}_j , and \bar{z}_j in (3) we see that $\bar{x}_{ij}, \bar{y}_{ij}$, and \bar{z}_{ij} are functions of x_j, y_j ,

and z_j , respectively. The chain rule can thus be used as

$$\begin{aligned} \frac{\partial \mathbf{B}_i}{\partial x_j} &= \frac{\partial \mathbf{B}_i}{\partial \bar{x}_{ij}} \frac{\partial \bar{x}_{ij}}{\partial x_j} + \frac{\partial \mathbf{B}_i}{\partial \bar{y}_{ij}} \frac{\partial \bar{y}_{ij}}{\partial x_j} + \frac{\partial \mathbf{B}_i}{\partial \bar{z}_{ij}} \frac{\partial \bar{z}_{ij}}{\partial x_j} \\ &= \frac{\partial \mathbf{B}_i}{\partial \bar{x}_{ij}} (-1) + \frac{\partial \mathbf{B}_i}{\partial \bar{y}_{ij}} (0) + \frac{\partial \mathbf{B}_i}{\partial \bar{z}_{ij}} (0) \end{aligned} \quad (10)$$

for x_j , and similarly for y_j and z_j , to get

$$\mathbf{J}_{ij} = \begin{bmatrix} -\frac{\partial}{\partial \bar{x}_{ij}} B_{ix} & -\frac{\partial}{\partial \bar{y}_{ij}} B_{ix} & -\frac{\partial}{\partial \bar{z}_{ij}} B_{ix} & \frac{\partial}{\partial \theta_j} B_{ix} & \frac{\partial}{\partial \phi_j} B_{ix} & \frac{\partial}{\partial \bar{m}_j} B_{ix} \\ -\frac{\partial}{\partial \bar{x}_{ij}} B_{iy} & -\frac{\partial}{\partial \bar{y}_{ij}} B_{iy} & -\frac{\partial}{\partial \bar{z}_{ij}} B_{iy} & \frac{\partial}{\partial \theta_j} B_{iy} & \frac{\partial}{\partial \phi_j} B_{iy} & \frac{\partial}{\partial \bar{m}_j} B_{iy} \\ -\frac{\partial}{\partial \bar{x}_{ij}} B_{iz} & -\frac{\partial}{\partial \bar{y}_{ij}} B_{iz} & -\frac{\partial}{\partial \bar{z}_{ij}} B_{iz} & \frac{\partial}{\partial \theta_j} B_{iz} & \frac{\partial}{\partial \phi_j} B_{iz} & \frac{\partial}{\partial \bar{m}_j} B_{iz} \end{bmatrix}. \quad (11)$$

These derivatives exist, and the analytic expressions for the elements of (11) are given by (11a)-(11r) below. These derivatives were calculated by hand and verified using a symbolic equation solver [30]. Because of the many repeated terms in (11a)-(11r), these elements are able to be efficiently calculated using common subexpression elimination.

The full $3N \times 6M$ Jacobian matrix is composed of all of the Jacobian submatrices \mathbf{J}_{ij} across the N sensors and M magnets, and is constructed as

$$\mathbf{J} = \begin{bmatrix} \mathbf{J}_{11} & \mathbf{J}_{12} & \dots & \mathbf{J}_{1M} \\ \mathbf{J}_{21} & \mathbf{J}_{22} & \dots & \mathbf{J}_{2M} \\ \vdots & \vdots & \ddots & \vdots \\ \mathbf{J}_{N1} & \mathbf{J}_{N2} & \dots & \mathbf{J}_{NM} \end{bmatrix}. \quad (12)$$

$$-\frac{\partial}{\partial \bar{x}_{ij}} B_{ix} = \bar{m}_j (\bar{x}_{ij}^2 + \bar{y}_{ij}^2 + \bar{z}_{ij}^2)^{-7/2} (3\bar{x}_{ij}(2\bar{x}_{ij}^2 - 3\bar{y}_{ij}^2 - 3\bar{z}_{ij}^2) \sin \theta_j \cos \phi_j + 3\bar{y}_{ij}(4\bar{x}_{ij}^2 - \bar{y}_{ij}^2 - \bar{z}_{ij}^2) \sin \theta_j \sin \phi_j + 3\bar{z}_{ij}(4\bar{x}_{ij}^2 - \bar{y}_{ij}^2 - \bar{z}_{ij}^2) \cos \theta_j) \quad (11a)$$

$$-\frac{\partial}{\partial \bar{x}_{ij}} B_{iy} = \bar{m}_j (\bar{x}_{ij}^2 + \bar{y}_{ij}^2 + \bar{z}_{ij}^2)^{-7/2} (3\bar{y}_{ij}(4\bar{x}_{ij}^2 - \bar{y}_{ij}^2 - \bar{z}_{ij}^2) \sin \theta_j \cos \phi_j + 3\bar{x}_{ij}(-\bar{x}_{ij}^2 + 4\bar{y}_{ij}^2 - \bar{z}_{ij}^2) \sin \theta_j \sin \phi_j + 15\bar{x}_{ij}\bar{y}_{ij}\bar{z}_{ij} \cos \theta_j) \quad (11b)$$

$$-\frac{\partial}{\partial \bar{x}_{ij}} B_{iz} = \bar{m}_j (\bar{x}_{ij}^2 + \bar{y}_{ij}^2 + \bar{z}_{ij}^2)^{-7/2} (3\bar{z}_{ij}(4\bar{x}_{ij}^2 - \bar{y}_{ij}^2 - \bar{z}_{ij}^2) \sin \theta_j \cos \phi_j + 15\bar{x}_{ij}\bar{y}_{ij}\bar{z}_{ij} \sin \theta_j \sin \phi_j + 3\bar{x}_{ij}(-\bar{x}_{ij}^2 - \bar{y}_{ij}^2 + 4\bar{z}_{ij}^2) \cos \theta_j) \quad (11c)$$

$$-\frac{\partial}{\partial \bar{y}_{ij}} B_{ix} = \bar{m}_j (\bar{x}_{ij}^2 + \bar{y}_{ij}^2 + \bar{z}_{ij}^2)^{-7/2} (3\bar{y}_{ij}(4\bar{x}_{ij}^2 - \bar{y}_{ij}^2 - \bar{z}_{ij}^2) \sin \theta_j \cos \phi_j + 3\bar{x}_{ij}(-\bar{x}_{ij}^2 + 4\bar{y}_{ij}^2 - \bar{z}_{ij}^2) \sin \theta_j \sin \phi_j + 15\bar{x}_{ij}\bar{y}_{ij}\bar{z}_{ij} \cos \theta_j) \quad (11d)$$

$$-\frac{\partial}{\partial \bar{y}_{ij}} B_{iy} = \bar{m}_j (\bar{x}_{ij}^2 + \bar{y}_{ij}^2 + \bar{z}_{ij}^2)^{-7/2} (3\bar{x}_{ij}(-\bar{x}_{ij}^2 + 4\bar{y}_{ij}^2 - \bar{z}_{ij}^2) \sin \theta_j \cos \phi_j + 3\bar{y}_{ij}(-3\bar{x}_{ij}^2 + 2\bar{y}_{ij}^2 - 3\bar{z}_{ij}^2) \sin \theta_j \sin \phi_j + 3\bar{z}_{ij}(-\bar{x}_{ij}^2 + 4\bar{y}_{ij}^2 - \bar{z}_{ij}^2) \cos \theta_j) \quad (11e)$$

$$-\frac{\partial}{\partial \bar{y}_{ij}} B_{iz} = \bar{m}_j (\bar{x}_{ij}^2 + \bar{y}_{ij}^2 + \bar{z}_{ij}^2)^{-7/2} (15\bar{x}_{ij}\bar{y}_{ij}\bar{z}_{ij} \sin \theta_j \cos \phi_j + 3\bar{z}_{ij}(-\bar{x}_{ij}^2 + 4\bar{y}_{ij}^2 - \bar{z}_{ij}^2) \sin \theta_j \sin \phi_j + 3\bar{y}_{ij}(-\bar{x}_{ij}^2 - \bar{y}_{ij}^2 + 4\bar{z}_{ij}^2) \cos \theta_j) \quad (11f)$$

$$-\frac{\partial}{\partial \bar{z}_{ij}} B_{ix} = \bar{m}_j (\bar{x}_{ij}^2 + \bar{y}_{ij}^2 + \bar{z}_{ij}^2)^{-7/2} (3\bar{z}_{ij}(4\bar{x}_{ij}^2 - \bar{y}_{ij}^2 - \bar{z}_{ij}^2) \sin \theta_j \cos \phi_j + 15\bar{x}_{ij}\bar{y}_{ij}\bar{z}_{ij} \sin \theta_j \sin \phi_j + 3\bar{x}_{ij}(-\bar{x}_{ij}^2 - \bar{y}_{ij}^2 + 4\bar{z}_{ij}^2) \cos \theta_j) \quad (11g)$$

$$-\frac{\partial}{\partial \bar{z}_{ij}} B_{iy} = \bar{m}_j (\bar{x}_{ij}^2 + \bar{y}_{ij}^2 + \bar{z}_{ij}^2)^{-7/2} (15\bar{x}_{ij}\bar{y}_{ij}\bar{z}_{ij} \sin \theta_j \cos \phi_j + 3\bar{z}_{ij}(-\bar{x}_{ij}^2 + 4\bar{y}_{ij}^2 - \bar{z}_{ij}^2) \sin \theta_j \sin \phi_j + 3\bar{y}_{ij}(-\bar{x}_{ij}^2 - \bar{y}_{ij}^2 + 4\bar{z}_{ij}^2) \cos \theta_j) \quad (11h)$$

$$-\frac{\partial}{\partial \bar{z}_{ij}} B_{iz} = \bar{m}_j (\bar{x}_{ij}^2 + \bar{y}_{ij}^2 + \bar{z}_{ij}^2)^{-7/2} (3\bar{x}_{ij}(-\bar{x}_{ij}^2 - \bar{y}_{ij}^2 + 4\bar{z}_{ij}^2) \sin \theta_j \cos \phi_j + 3\bar{y}_{ij}(-\bar{x}_{ij}^2 - \bar{y}_{ij}^2 + 4\bar{z}_{ij}^2) \sin \theta_j \sin \phi_j + 3\bar{z}_{ij}(-3\bar{x}_{ij}^2 - 3\bar{y}_{ij}^2 + 2\bar{z}_{ij}^2) \cos \theta_j) \quad (11i)$$

$$\frac{\partial}{\partial \theta_j} B_{ix} = \bar{m}_j (\bar{x}_{ij}^2 + \bar{y}_{ij}^2 + \bar{z}_{ij}^2)^{-5/2} ((2\bar{x}_{ij}^2 - \bar{y}_{ij}^2 - \bar{z}_{ij}^2) \cos \phi_j \cos \theta_j + 3\bar{x}_{ij}\bar{y}_{ij} \sin \phi_j \cos \theta_j - 3\bar{x}_{ij}\bar{z}_{ij} \sin \theta_j) \quad (11j)$$

$$\frac{\partial}{\partial \theta_j} B_{iy} = \bar{m}_j (\bar{x}_{ij}^2 + \bar{y}_{ij}^2 + \bar{z}_{ij}^2)^{-5/2} (3\bar{x}_{ij}\bar{y}_{ij} \cos \phi_j \cos \theta_j + (-\bar{x}_{ij}^2 + 2\bar{y}_{ij}^2 - \bar{z}_{ij}^2) \sin \phi_j \cos \theta_j - 3\bar{y}_{ij}\bar{z}_{ij} \sin \theta_j) \quad (11k)$$

$$\frac{\partial}{\partial \theta_j} B_{iz} = \bar{m}_j (\bar{x}_{ij}^2 + \bar{y}_{ij}^2 + \bar{z}_{ij}^2)^{-5/2} (3\bar{x}_{ij}\bar{z}_{ij} \cos \phi_j \cos \theta_j + 3\bar{y}_{ij}\bar{z}_{ij} \sin \phi_j \cos \theta_j - (-\bar{x}_{ij}^2 - \bar{y}_{ij}^2 + 2\bar{z}_{ij}^2) \sin \theta_j) \quad (11l)$$

$$\frac{\partial}{\partial \phi_j} B_{ix} = \bar{m}_j (\bar{x}_{ij}^2 + \bar{y}_{ij}^2 + \bar{z}_{ij}^2)^{-5/2} (3\bar{x}_{ij}\bar{y}_{ij} \sin \theta_j \cos \phi_j - (2\bar{x}_{ij}^2 - \bar{y}_{ij}^2 - \bar{z}_{ij}^2) \sin \theta_j \sin \phi_j) \quad (11m)$$

$$\frac{\partial}{\partial \phi_j} B_{iy} = \bar{m}_j (\bar{x}_{ij}^2 + \bar{y}_{ij}^2 + \bar{z}_{ij}^2)^{-5/2} ((-\bar{x}_{ij}^2 + 2\bar{y}_{ij}^2 - \bar{z}_{ij}^2) \sin \theta_j \cos \phi_j - 3\bar{x}_{ij}\bar{y}_{ij} \sin \theta_j \sin \phi_j) \quad (11n)$$

$$\frac{\partial}{\partial \phi_j} B_{iz} = \bar{m}_j (\bar{x}_{ij}^2 + \bar{y}_{ij}^2 + \bar{z}_{ij}^2)^{-5/2} (3\bar{y}_{ij}\bar{z}_{ij} \sin \theta_j \cos \phi_j - 3\bar{x}_{ij}\bar{z}_{ij} \sin \theta_j \sin \phi_j) \quad (11o)$$

$$\frac{\partial}{\partial \bar{m}_j} B_{ix} = (\bar{x}_{ij}^2 + \bar{y}_{ij}^2 + \bar{z}_{ij}^2)^{-5/2} ((2\bar{x}_{ij}^2 - \bar{y}_{ij}^2 - \bar{z}_{ij}^2) \sin \theta_j \cos \phi_j + 3\bar{x}_{ij}\bar{y}_{ij} \sin \theta_j \sin \phi_j + 3\bar{x}_{ij}\bar{z}_{ij} \cos \theta_j) \quad (11p)$$

$$\frac{\partial}{\partial \bar{m}_j} B_{iy} = (\bar{x}_{ij}^2 + \bar{y}_{ij}^2 + \bar{z}_{ij}^2)^{-5/2} (3\bar{x}_{ij}\bar{y}_{ij} \sin \theta_j \cos \phi_j + (-\bar{x}_{ij}^2 + 2\bar{y}_{ij}^2 - \bar{z}_{ij}^2) \sin \theta_j \sin \phi_j + 3\bar{y}_{ij}\bar{z}_{ij} \cos \theta_j) \quad (11q)$$

$$\frac{\partial}{\partial \bar{m}_j} B_{iz} = (\bar{x}_{ij}^2 + \bar{y}_{ij}^2 + \bar{z}_{ij}^2)^{-5/2} (3\bar{x}_{ij}\bar{z}_{ij} \sin \theta_j \cos \phi_j + 3\bar{y}_{ij}\bar{z}_{ij} \sin \theta_j \sin \phi_j + (-\bar{x}_{ij}^2 - \bar{y}_{ij}^2 + 2\bar{z}_{ij}^2) \cos \theta_j) \quad (11r)$$

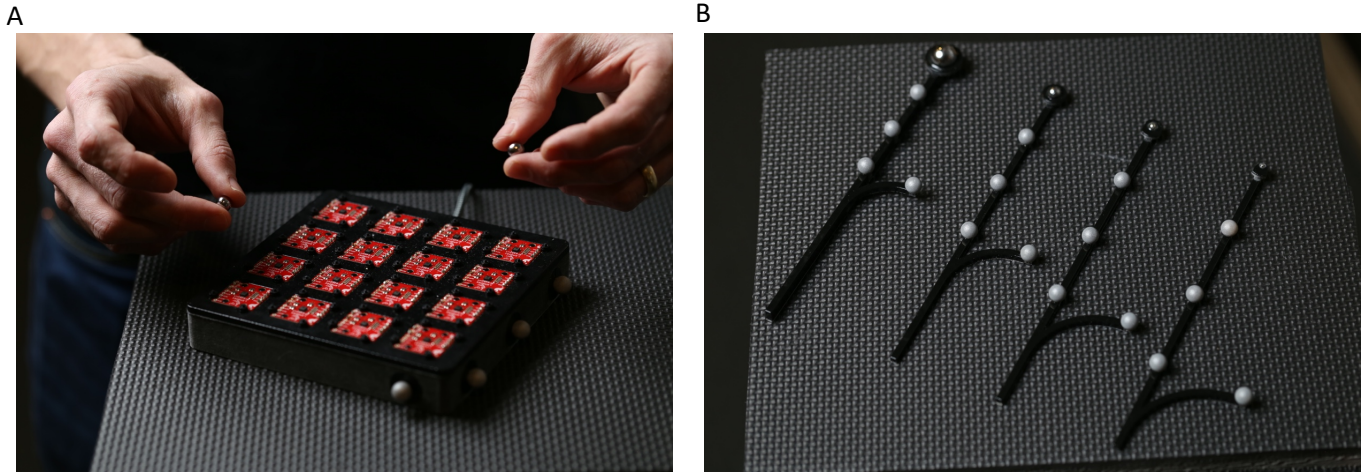


Fig. 1. **4x4 Grid of Magnetometers and Tracking Wands with Magnets.** (A) A 4x4 magnetometer array was created using a 3d-printed structure with reflective markers for tracking. (B) Each magnet was attached north-pole-up to a unique 3d-printed wand with reflective markers for tracking.

3) *Disturbance Field Compensation:* Assuming that there is a uniform disturbance field seen across all magnetic field sensors (from, for example, the geomagnetic field), its Jacobian submatrix would be given by

$$\begin{aligned} \mathbf{D}_i &= \begin{bmatrix} \frac{\partial}{\partial G_x} B_{ix} & \frac{\partial}{\partial G_y} B_{ix} & \frac{\partial}{\partial G_z} B_{ix} \\ \frac{\partial}{\partial G_x} B_{iy} & \frac{\partial}{\partial G_y} B_{iy} & \frac{\partial}{\partial G_z} B_{iy} \\ \frac{\partial}{\partial G_x} B_{iz} & \frac{\partial}{\partial G_y} B_{iz} & \frac{\partial}{\partial G_z} B_{iz} \end{bmatrix} \\ &= \begin{bmatrix} 1 & 0 & 0 \\ 0 & 1 & 0 \\ 0 & 0 & 1 \end{bmatrix} = \mathbf{I}_3, \end{aligned} \quad (13)$$

the 3x3 identity matrix. The columns of the Jacobian submatrix corresponding to the disturbance field are thus given by

$$\mathbf{D} = \begin{bmatrix} \mathbf{I}_3 \\ \mathbf{I}_3 \\ \vdots \\ \mathbf{I}_3 \end{bmatrix}, \quad (14)$$

a $3N \times 3$ matrix. Extending the Jacobian matrix (12) with the result in (14), we get the augmented Jacobian matrix

$$\hat{\mathbf{J}} = [\mathbf{J} \mid \mathbf{D}]. \quad (15)$$

This augmented matrix assists in providing robust tracking information under sensor motion or far-field disturbance.

4) *Calibration:* The sensor array was calibrated using rotation in a uniform ambient field to remove offsets and distortions [31], [32], and then the sensors were scaled relative to one another to achieve equivalent full-scale ranges. Spike noise was filtered out using a three-point median filter.

B. Hardware

The tracking algorithm was written in C++ and implemented an unconstrained Levenberg-Marquardt algorithm via C/C++ Minpack [33]. The algorithm was run in real-time on a

Macbook Air (13-inch, Early 2014) with 8 GB of RAM and an Intel i7 CPU running at 1.7 GHz.

The three-axis magnetic field was measured using 16 LSM9DS1 iNEMO inertial modules (STMicroelectronics) at a sampling rate of 1 kHz. The measurements were communicated via SPI (10 MHz clock) to a Teensy 3.6 microcontroller (PJRC) and relayed to the Macbook Air via USB.

Spherical chrome-plated neodymium magnets (SuperMagnetMan) were used in this study, with diameters 2 mm (SP0200), 4 mm (SP0400), 8 mm (SP100352), and 16 mm (SP1062). Four 8 mm diameter magnets were used to validate the tracking of multiple magnets at once. The magnetic dipole strength of each magnet was measured by tracking it with six degrees of freedom (including the magnetic dipole strength), after which the median of the tracked dipole strength was used as the known magnetic dipole strength for five-degree-of-freedom tracking.

A Connex 500 printer (Stratasys) was used to print a flat 4x4 grid (100mm by 100mm) for the magnetic field sensors (see Fig. 1A) and one unique tracking wand for each of the permanent magnets (see Fig. 1B). The sensor array and magnet wands were each marked with four 9.5 mm Reflective Pearl Markers (B&L Engineering). Seven T40S infrared cameras (Vicon Motion Systems), calibrated to an average resolution of 31 μm (standard deviation of 9 μm) were used to track the sensor array and magnets.

C. Experiments

To test the latency, accuracy, and disturbance compensation of our algorithm, we first fixed the sensor array in position and orientation to maintain a consistent ambient disturbance field. Motion capture tracking wands were then used to manually move the one or more magnets over the sensor array, varying position and orientation, for one minute. In all cases, disturbance compensation was used while tracking the magnets.

1) *Magnet Tracking Latency*: To compare the latency of tracking methods using a numerical, an analytic, and a code-optimized Jacobian matrix, one, two, three, and then four 8 mm diameter magnets were simultaneously tracked in real time using the code-optimized Jacobian matrix method. All raw magnetic field data was saved and used to re-track the magnets offline with the non-code-optimized-analytic and numerical Jacobian matrix tracking methods. This provided a one-to-one comparison of tracking latencies for the given inputs.

2) *Magnet Tracking Accuracy*: Separate tracking sessions were used to individually track a 2 mm, a 4 mm, an 8 mm, and a 16 mm diameter magnet. For each of these magnets tracked individually, as well as for the four 8 mm diameter magnets tracked simultaneously, reflective marker positions were used in post-processing to determine the positions and orientations of the magnets relative to the magnetometer array. These positions and orientations were then compared against the positions and orientations predicted in real time by the magnetometer array.

For each magnet, positions and position errors were then normalized by dividing by the magnet's radius. To demonstrate the utility of this normalization, we multiply the first and second summation terms of (8) by $\frac{1}{R_{j'}^5} / \frac{1}{R_{j'}^5}$ and $\frac{1}{R_{j'}^3} / \frac{1}{R_{j'}^3}$, respectively, to get

$$\mathbf{B}_i = \mathbf{G} + \sum_{j'=0}^{j'=M} \left(\frac{3 \frac{\mathbf{r}_{ij'}}{R_{j'}} \left(\frac{\hat{\mathbf{m}}_{j'}^T}{R_{j'}} \cdot \frac{\mathbf{r}_{ij'}}{R_{j'}} \right)}{\left(\frac{r_{ij'}}{R_{j'}} \right)^5} - \frac{\frac{\hat{\mathbf{m}}_{j'}}{R_{j'}^3}}{\left(\frac{r_{ij'}}{R_{j'}} \right)^3} \right). \quad (16)$$

Defining the unit magnetic moment vector $\hat{\mathbf{m}}_j \triangleq \frac{\hat{\mathbf{m}}_j}{m_j}$ and using (7) gives $\frac{\hat{\mathbf{m}}_j}{R_j^3} = \frac{B_{rj}}{3} \hat{\mathbf{m}}_j$. If we then define the dimensionless relative position vector $\check{\mathbf{r}}_{ij} \triangleq \frac{\mathbf{r}_{ij}}{R_j}$, we can simplify (16) as

$$\mathbf{B}_i = \mathbf{G} + \sum_{j'=0}^{j'=M} B_{rj'} \left(\frac{\check{\mathbf{r}}_{ij'} (\hat{\mathbf{m}}_{j'}^T \cdot \check{\mathbf{r}}_{ij'})}{\check{r}_{ij'}^5} - \frac{\hat{\mathbf{m}}_{j'}}{3 \check{r}_{ij'}^3} \right), \quad (17)$$

demonstrating that the magnetic field from a magnet-magnetometer system is scale invariant. Thus, magnet-magnetometer systems with equivalent normalized sensor and magnet positions will, given the same sensor noise, produce the same normalized position error

$$\check{e}_{p_j} = \frac{e_{p_j}}{R_j}. \quad (18)$$

This scale invariance does require, however, that the residual flux densities $B_{rj'}$ in (17) be equivalent from one system to the next. To compare our different normalized magnet-magnetometer systems, we define a reference residual flux density, which we will fix arbitrarily as $B_{rref} = 1.2$ T. Rearranging (7) with this reference residual flux density, we can fully represent the strength of a magnet by its equivalent radius, as

$$R_{eq_j} = \sqrt[3]{\frac{3\hat{m}_j}{B_{rref}}}. \quad (19)$$

Equation (19) was used to determine the radius of each magnet and (18) was used to normalize the position error. Orientation error and normalized position error were then plotted against the normalized average distance of each magnet,

$$\check{r}_{avg_j} = \frac{1}{N} \sum_{i=1}^N \|\check{\mathbf{r}}_{ij}\|, \quad (20)$$

where N is the number of sensors. This is the average linear distance from a given magnet to all of the sensors, normalized by dividing by the equivalent radius of the tracked magnet.

The common logarithm was applied to the orientation and normalized position errors, and Stata 15.1 [34] was used to fit a linear regression of log error versus normalized average distance from sensors, using the robust option to account for heteroskedasticity in the standard errors.

3) *Disturbance Tracking Accuracy*: In the absence of any magnets, the ambient disturbance field was measured for one minute on all of the sensors. This ambient field data was then temporally and spatially averaged to give a measured disturbance field vector, $\tilde{\mathbf{G}} = (\tilde{G}_x, \tilde{G}_y, \tilde{G}_z)$. For a given sample, the disturbance field tracking error e_G was then calculated against this measured disturbance field as

$$e_G = \frac{\|\mathbf{G} - \tilde{\mathbf{G}}\|}{\|\tilde{\mathbf{G}}\|}. \quad (21)$$

III. RESULTS

A. Magnet Tracking Latency

Using an analytically computed Jacobian matrix, multiple magnets were tracked simultaneously with low tracking latency while compensating for a magnetic disturbance field (see supplemental video for a demonstration of the tracking). Fig. 2 displays these results, showing tracking latency plotted versus degrees of freedom. Tracking latency is defined here as the time required to determine the position of one or more magnets once the magnetic field measurements are known. The number of degrees of freedom is the total number of estimated parameters for all tracked magnets (not including the number of parameters needed to track the disturbance field). For instance, a magnet of known dipole strength has five degrees of freedom, two magnets of known strength together have ten degrees of freedom, and four magnets of known strength and known orientation, but unknown position, together have twelve degrees of freedom. To create a benchmark for comparison, we searched the literature for all magnet tracking applications where latency was reported. Wherever latency was not reported, we inverted the magnet-tracking sampling rate as a proxy for latency. Otherwise, latencies are reported as given or using the 90th percentile latency of the reported values. We also note that the comparison is limited by a lack of data on computing systems used for tracking, so the latencies from past work are reported for baseline reference only. These tracking latencies from past literature [1], [8], [16], [24], [25], [35]–[44] are shown in Fig. 2. Only latencies from real-time physical magnet tracking are included.

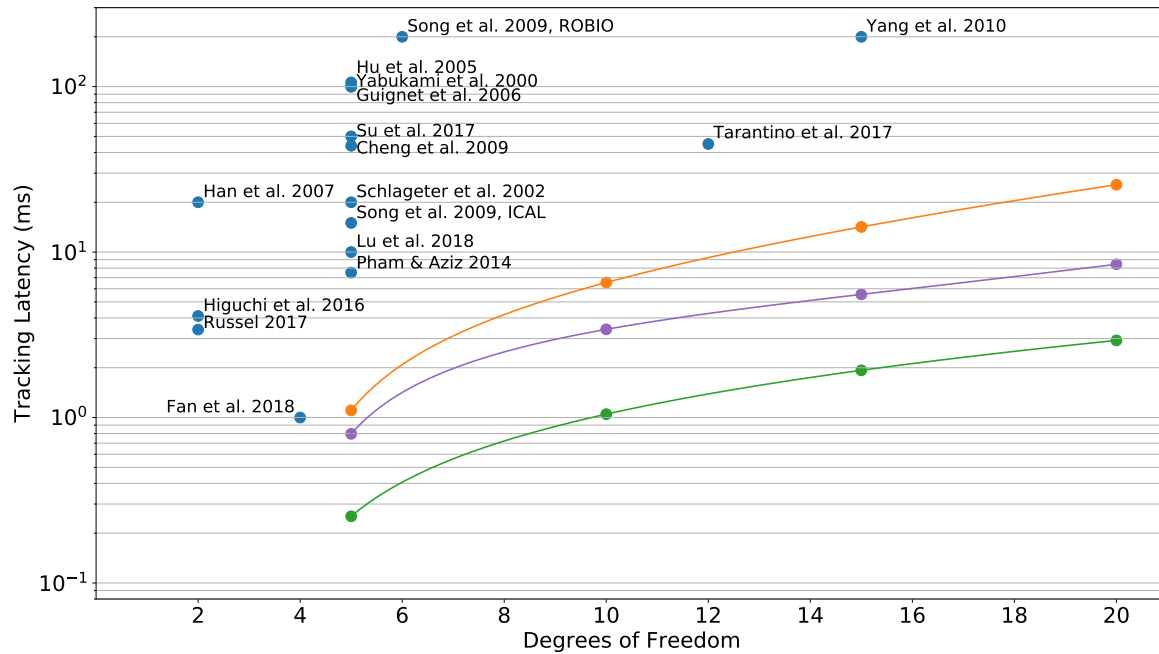


Fig. 2. **Comparison of Tracking Latencies.** When tracking one to four magnets, each with five degrees of freedom, analytically calculating the gradient of optimization error results in a reduced 90th-percentile tracking latency (plotted in purple) in magnet tracking when compared to numerical calculation of the gradient (plotted in orange). A further drop in latency is observed when the analytic calculation of the gradient is implemented with common subexpression elimination (plotted in green). Tracking latencies (blue) from past work are plotted for reference. Trends are indicated by cubic splines. See Fig. 6 in the appendix for the distribution of latencies.

To establish an experimentally relevant baseline for the tracking latency, we utilized a traditionally-implemented algorithm, the Levenberg-Marquardt algorithm, with a numerical Jacobian matrix to track one to four magnets with disturbance compensation. In relation to previous work where similar computing power is used, we attribute the improvement in latency of this new baseline to our use of a compiled language. Implementing this same algorithm with an analytically-computed Jacobian matrix, we found a large increase in speed (see Fig. 2). For 1, 2, 3 and 4 magnets (5, 10, 15, and 20 degrees of freedom), the use of an analytic Jacobian matrix increases the maximum bandwidth by 39%, 92%, 156%, and 202%, respectively. Implementing this same algorithm again using common subexpression elimination in the calculation of the analytic Jacobian matrix, we found an even larger increase in maximum bandwidth of 336%, 525%, 635%, and 773% for 1, 2, 3 and 4 magnets, respectively.

B. Tracking Accuracy for Individual Magnets

The same cost function is optimized whether by numerical or analytic calculation of the Jacobian, so the tracking error is unchanged between one method of calculation and the other. We wished to characterize this tracking error with our system for various magnet diameters. Tracking error as a function of height has been addressed in the literature [45], but there is currently no standard for comparing errors across differing sensor array geometries as well as differing magnet

strengths, orientations, and general positions relative to the sensor array. Using the average distance from all sensors to each magnet allows us to characterize the error while condensing these dimensions, with temporal variance in sensor noise resulting in a distribution of tracking accuracy for a given magnet position. With this characterization, Fig. 3A shows the measured accuracy of our system, whereas Fig. 3B shows a real time trajectory from the magnet tracking compared against state-of-the-art motion capture. As discussed in section II-C2, the position errors and average distance from sensors in Fig. 3A are normalized by the radius of each magnet.

C. Tracking Accuracy for Multiple Magnets

To test the accuracy of tracking multiple magnets at once, we applied this same error characterization to the tracking of multiple magnets. Fig. 4 shows this error characterization applied to the simultaneous tracking of four 8 mm diameter magnets.

D. Magnetic Disturbance Field Tracking

We were interested in whether our algorithm could detect a spatially uniform disturbance field without prior information about the ambient field. To verify this, the algorithm was initialized at the start of tracking with a disturbance estimate of zero. The disturbance was then tracked and recorded while tracking individual magnets with diameters 2 mm, 4 mm,

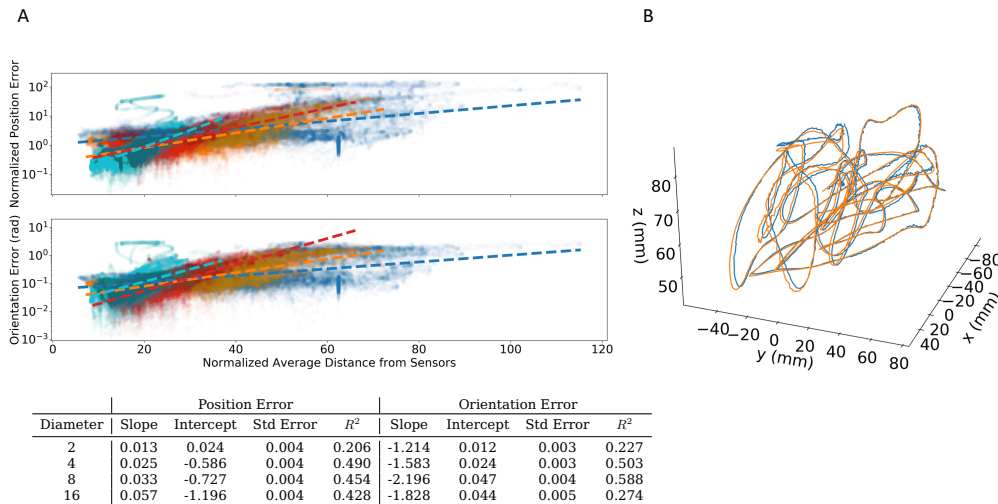


Fig. 3. **Empirical Position and Orientation Accuracy for Separate Magnets.** (A) Orientation and normalized position errors are plotted versus the normalized average distance from each magnet to all magnetic field sensors, for 2 mm, 4 mm, 8 mm, and 16 mm diameter magnets (shown in blue, orange, red, and cyan, respectively). For each magnet, the position errors and the average distances are normalized by dividing by the magnet's radius. These errors represent the errors from a single magnet being tracked. Linear regression information on the common log of the errors, with standard errors, is supplied to describe the variance of the data. (B) A representative five-second time interval is shown when tracking an 8 mm diameter magnet (shown in blue) versus motion capture (shown in orange).

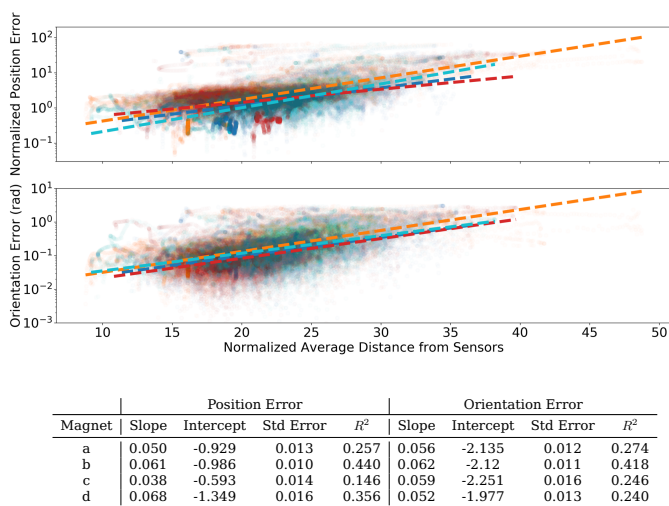


Fig. 4. **Empirical Position and Orientation Accuracy for Four Magnets Tracked Together.** For four 8 mm diameter magnets tracked simultaneously, the orientation and normalized position errors are plotted versus the normalized average distance from each magnet to all magnetic field sensors (blue, orange, red, and cyan for magnets a, b, c, and d respectively). For each magnet, the position errors and the average distances are normalized by dividing by the magnet radius. Linear regression information on the common log of the errors, with standard errors, is provided to describe the variance of the data. The errors correspond to each individual 8 mm diameter magnet as the four magnets are tracked simultaneously (compare with the 8 mm diameter magnet tracked individually in Fig. 3A).

8 mm, and 16 mm, as well as while tracking two, three, and four 8 mm magnets simultaneously (see Fig. 5). When tracking magnetic disturbances for the individual magnets with diameters 2 mm, 4 mm, 8 mm, and 16 mm, the mean errors of the magnetic disturbances were 1.25%, 1.24%, 2.52%, and

8.92%, respectively. While tracking two, three, and four 8 mm magnets simultaneously, the mean errors were 4.00%, 5.90%, and 7.93%, respectively. In summary, the algorithm was able to successfully track disturbances in real time for individual magnets ranging from 2 mm to 16 mm in size, as well as for simultaneous tracking of four magnets at the fixed size of 8 mm. These results underscore the applicability of the algorithm for the cancellation of magnetic disturbance fields in mobile applications comprising magnets of different size and number.

IV. DISCUSSION

A. Analysis of Results

Our objective was to show that multiple magnets can be tracked with low latency for mobile tracking applications and to characterize the error associated with our magnet tracking system. The tracking latency of this algorithm increases as $\mathcal{O}(M^3 + M^2N)$, where M is the number of magnets and N is the number of sensors [46]. Thus, though Fig. 2 shows how tracking latency increases with number of magnets, additional sensors would also increase the tracking latency. Tracking error on the other hand, typically decreases with an increasing number of sensors [38], resulting in a trade-off between tracking latency and tracking error. As reflected in Figs. 3 and 4, sensor noise limits the distance from the sensing array because of decreased signal-to-noise ratio, due chiefly to Johnson and flicker noise from the magnetic field sensors.

At closer range, tracking error is more dependent upon the validity of the dipole model. The dipole model can be applied to nonspherical magnets with differing levels of accuracy [47], but we have chosen to track spherical magnets because, when magnetized uniformly, they are exactly described as

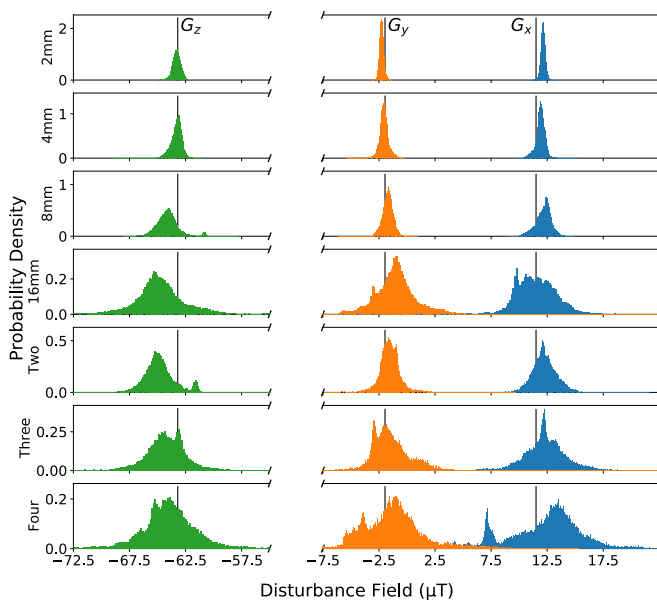


Fig. 5. **Measured vs. Tracked Disturbance.** Vertical black lines describe the magnetic field disturbance as measured before the introduction of permanent magnets to the system. The distributions describe the three components of magnetic field disturbance (blue, orange and green for disturbance in the x, y, and z directions, respectively) as tracked by the algorithm for the individual magnets with diameters 2 mm, 4 mm, 8 mm, and 16 mm, as well as while tracking two, three and four 8 mm diameter magnets simultaneously.

dipoles [17]. However, in practice permanent magnets are not magnetized with perfect uniformity. This magnetization inhomogeneity causes the field from a magnetic sphere to differ from that of a perfect dipole, and this contributes to the tracking error observed close to the sensor array.

In Figs. 3 and 4, linear fits of the common log of the errors, with standard errors, represent the error as distance from the sensing array increases. The intercepts roughly suggest the best accuracy that can be achieved with the given sensor geometry and sensor noise level, though in practice zero average distance to all sensors cannot be achieved. The slopes of these linear fits represent how error increases as distance from the array increases. Normalized magnet-magnetometer systems corresponding to smaller magnet radii have lower slopes but higher intercepts, suggesting that sensor array geometries of greater normalized width (i.e., those corresponding to sensors that are farther apart or magnets that are smaller) allow a larger tracking volume for a given minimum accuracy at the cost of reduced maximum accuracy.

As shown in Fig. 4, when tracking four magnets at once the linear regression fits of the log error have higher slopes, but the intercepts are still low. This suggests that multiple magnets can be tracked with high accuracies at close range using this algorithm, but that with multiple magnets the accuracy drops more quickly as the magnets are moved away from the sensors.

When tracking the disturbance field (see Fig. 5), the algorithm was not initialized with any information about the ambient field. This shows that the tracking algorithm is able to detect in real time a spatially uniform disturbance field without prior knowledge of the field. Though a static sensor array configuration was used for validating accuracy in this investigation, the algorithm is capable in principle of tracking

the disturbance field even when the sensor array varies in position and orientation and the field varies temporally. Such tracking robustness suggests this algorithm can be applied to mobile applications.

B. Applications

This work makes possible new high-bandwidth applications for magnet tracking. For example, real-time high-bandwidth magnet tracking enables improved position feedback for closed-loop control, such as for robotics, multi-degree-of-freedom magnetic levitation, low-latency augmented and virtual reality human-computer interaction, and high-fidelity control of prostheses and exoskeletons. Further, this work can be applied to real-time body motion capture using multi-degree-of-freedom magnet-based goniometry at multiple joints, or to detailed facial tracking using a large number of small magnets.

C. Limitations and Future Work

This work is limited to five-degree-of-freedom pose tracking for each magnet. This is because the magnetic field of an axially symmetric magnet is also axially symmetric, and thus its orientation can be specified from its magnetic field with no more than two parameters. Previous work demonstrates six-degree-of-freedom pose tracking using multiple non-symmetrically attached magnets on a rigid object [48]. The implementation of an analytic Jacobian matrix for six-degree-of-freedom pose tracking via constrained equations is an important area of future work and has immediate applications to tool-tracking in augmented and virtual reality. Previous work has also shown six-degree-of-freedom tracking of a sensor array relative to a single magnet, but this requires the use of an inertial measurement unit (IMU) [49]. Using multiple non-symmetrically fixed magnets, as in [48], a sensor array could be tracked without the need for an IMU. For applications where tracked devices can be powered, this would facilitate the independent high-speed tracking of several sensor arrays without a marginal cost in tracking latency.

This work is also limited to the tracking of spherical magnets or to the tracking of nonspherical magnets at far field. To accurately track nonspherical cylindrically-symmetric magnets (e.g., axially-magnetized cylinders) at close range, the use of higher order multipole expansions should be used. Previous work has implemented an analytic Jacobian corresponding to higher-order multipole expansions, but their derivation requires a zenith-length constraint which may affect the optimization convergence [29]. It should be investigated whether or not these higher-order multipole expansions can be reparametrized in terms of two orientation parameters. If so, it is expected that common subexpression elimination could be applied to these higher-order multipole expansions to achieve similar improvements in real-time tracking bandwidth.

Because the algorithm attempts to fit both a uniform field and one or more dipole fields to the magnetic field data, the uniform component of the magnetic field not accounted for by the dipole models is erroneously seen as part of the disturbance field. The size of this magnetic field not accounted for by the dipole model increases with increasing magnet diameter for a

given percent error in magnetic dipole strength measurement, as well as for a given magnetization inhomogeneity. As seen in Fig. 5, this means that larger magnet diameters result in larger deviations in the predicted disturbance field. This suggests that this work is limited in the accuracy of its measurement of magnetic dipole strength. The accuracy of the magnetic dipole strength measurement could be improved by combining multiple magnetic field measurements into a single optimization, as in [50].

The disturbance compensation implemented here assumes that the magnetic disturbance field is spatially uniform, so the spatially nonuniform components of the disturbance were not accounted for. These nonlinear components could be corrected for by introducing spatial gradient terms in each dimension (at the cost of higher complexity), but the effect of nonlinear disturbance compensation on tracking accuracy would need to be investigated.

This work did not investigate the tracking of multiple magnets of different sizes, nor did it investigate the tracking accuracies or tracking latencies associated with different numbers of sensors or different sensor geometries. In particular, optimal sensor geometries should be a focus of future investigation.

V. CONCLUSION

In this paper we derived the analytic Jacobian matrix for magnetic dipoles and demonstrated a dramatic increase in magnet tracking bandwidth without compromising for accuracy. This increase in bandwidth allows for the tracking of multiple magnets in real time while compensating for ambient magnetic field disturbances. While, at near field, this method only tracks with high accuracy for spherical magnets, we hope that future researchers can leverage our derivation to develop high-bandwidth magnet tracking algorithms for other magnet geometries.

APPENDIX

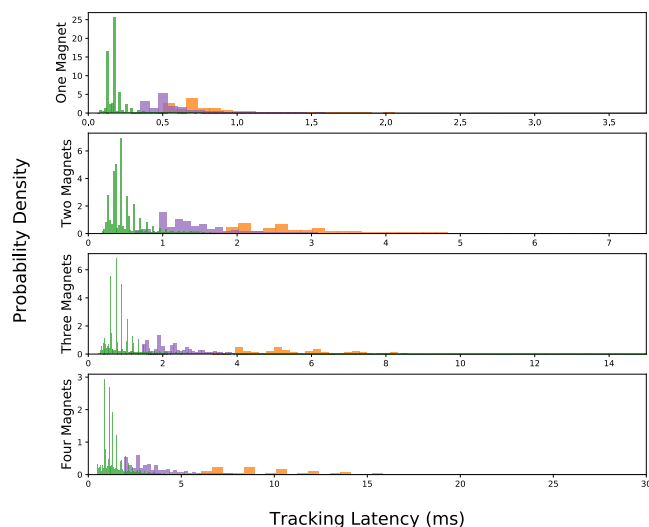


Fig. 6. **Tracking latencies for simultaneous tracking of one to four magnets.** Tracking latencies are shown for tracking one, two, three, and four magnets at once. Histograms represent tracking using Jacobian matrices calculated numerically (orange), analytically (purple), and utilizing common subexpression elimination (green).

ACKNOWLEDGEMENTS

The authors thank Tyler Clites, Jimmy Day, Bruce Deffenbaugh, Brian Mayton, Michael Nawrot, Shriya Srinivasan and Roman Stolyarov for their helpful guidance on the preparation and writing of this manuscript.

REFERENCES

- [1] X. Han, H. Seki, and M. Hikizu, "Wearable handwriting input device using magnetic field," in *SICE, 2007 Annual Conference*. IEEE, 2007, pp. 365–368.
- [2] Y. Ma, Z.-H. Mao, W. Jia, C. Li, J. Yang, and M. Sun, "Magnetic hand tracking for human-computer interface," *IEEE Transactions on Magnetics*, vol. 47, no. 5, pp. 970–973, 2011.
- [3] R.-H. Liang, K.-Y. Cheng, C.-H. Su, C.-T. Weng, B.-Y. Chen, and D.-N. Yang, "Gaussense: attachable stylus sensing using magnetic sensor grid," in *Proceedings of the 25th annual ACM symposium on User interface software and technology*. ACM, 2012, pp. 319–326.
- [4] D. Ashbrook, P. Baudisch, and S. White, "Nenya: subtle and eyes-free mobile input with a magnetically-tracked finger ring," in *Proceedings of the SIGCHI Conference on Human Factors in Computing Systems*. ACM, 2011, pp. 2043–2046.
- [5] Y. Chen, A. Mazumdar, C. F. Brooks, B. G. van Bloemen Waanders, S. D. Bond, and M. B. Nemer, "Remote distributed vibration sensing through opaque media using permanent magnets," *IEEE Transactions on Magnetics*, vol. 54, no. 6, pp. 1–13, 2018.
- [6] M. Wenger, E. Henderson, and J. Dinning, "Magnetometer method for recording gastric motility," *Science (Washington)*, vol. 125, pp. 990–991, 1957.
- [7] K. M. Popek, A. W. Mahoney, and J. J. Abbott, "Localization method for a magnetic capsule endoscope propelled by a rotating magnetic dipole field," in *2013 IEEE International Conference on Robotics and Automation*. IEEE, 2013, pp. 5348–5353.
- [8] Z. Sun, L. Maréchal, and S. Foong, "Passive magnetic-based localization for precise untethered medical instrument tracking," *Computer Methods and Programs in Biomedicine*, 2017.
- [9] Y. Sonoda, "Observation of tongue movements employing magnetometer sensor," *IEEE Transactions on Magnetics*, vol. 10, no. 3, pp. 954–957, 1974.
- [10] W. D. McCall and E. J. Rohan, "A linear position transducer using a magnet and hall effect devices," *IEEE Transactions on Instrumentation and Measurement*, vol. 26, no. 2, pp. 133–136, 1977.
- [11] J. A. Woltjen, G. W. Timm, F. M. Waltz, and W. E. Bradley, "Bladder motility detection using the hall effect," *IEEE Transactions on Biomedical Engineering*, no. 4, pp. 295–299, 1973.
- [12] J. A. Baldoni and B. B. Yellen, "Magnetic tracking system: Monitoring heart valve prostheses," *IEEE transactions on magnetics*, vol. 43, no. 6, pp. 2430–2432, 2007.
- [13] B. Smith, Z. Tang, M. W. Johnson, S. Pourmehdi, M. M. Gazdik, J. R. Buckett, and P. H. Peckham, "An externally powered, multichannel, implantable stimulator-telemeter for control of paralyzed muscle," *IEEE Transactions on Biomedical Engineering*, vol. 45, no. 4, pp. 463–475, 1998.
- [14] E. J. Rouse, D. C. Nahlik, M. A. Peshkin, and T. A. Kuiken, "Development of a model osseo-magnetic link for intuitive rotational control of upper-limb prostheses," *IEEE Transactions on Neural Systems and Rehabilitation Engineering*, vol. 19, no. 2, pp. 213–220, 2011.
- [15] N. Bhadra, P. H. Peckham, M. W. Keith, K. L. Kilgore, F. Montague, M. Gazdik, and T. Stage, "Implementation of an implantable joint-angle transducer," *Journal of rehabilitation research and development*, vol. 39, no. 3, pp. 411–422, 2002.
- [16] S. Tarantino, F. Clemente, D. Barone, M. Controzzi, and C. Cipriani, "The myokinetic control interface: tracking implanted magnets as a means for prosthetic control," *Scientific reports*, vol. 7, no. 1, p. 17149, 2017.
- [17] J. D. Jackson, "Classical electrodynamics," pp. 186,198, 1999.
- [18] D. Son, S. Yim, and M. Sitti, "A 5-d localization method for a magnetically manipulated untethered robot using a 2-d array of hall-effect sensors," *IEEE/ASME Transactions on Mechatronics*, vol. 21, no. 2, pp. 708–716, 2016.
- [19] S. V. Marshall, "Vehicle detection using a magnetic field sensor," *IEEE transactions on vehicular technology*, vol. 27, no. 2, pp. 65–68, 1978.
- [20] W. Eichhorn, "Magnetic dipole moment determination by near-field analysis," National Aeronautics and Space Administration, Greenbelt, MD, Tech. Rep., 1972.

- [21] A. S. Gadre, D. J. Stilwell, and B. Davis, "An information-theoretic approach to underwater magnetic dipole localization," in *OCEANS, 2005. Proceedings of MTS/IEEE*. IEEE, 2005, pp. 703–710.
- [22] D. Thompson, "Euldph: A new technique for making computer-assisted depth estimates from magnetic data," *Geophysics*, vol. 47, no. 1, pp. 31–37, 1982.
- [23] J. McFee and Y. Das, "Determination of the parameters of a dipole by measurement of its magnetic field," *IEEE Transactions on Antennas and Propagation*, vol. 29, no. 2, pp. 282–287, 1981.
- [24] M. Russel, "A Neural Network Driven Sensor Array for Locating a Permanent Magnet," PhD Thesis, University of Calgary, 2017.
- [25] W. Yang, C. Hu, M. Li, M. Q.-H. Meng, and S. Song, "A new tracking system for three magnetic objectives," *IEEE Transactions on Magnetics*, vol. 46, no. 12, pp. 4023–4029, 2010.
- [26] Y.-J. Ryoo, E.-S. Kim, Y.-C. Lim, Y.-H. Chang, C.-J. Moon, and S.-H. Yang, "Cancellation of background field using magnetic compass sensor for magnetometer based autonomous vehicle," in *SENSORS, 2003 IEEE*, vol. 1. IEEE, 2003, pp. 52–57.
- [27] W. Weitschies, O. Kosch, H. Mönnikes, and L. Trahms, "Magnetic marker monitoring: an application of biomagnetic measurement instrumentation and principles for the determination of the gastrointestinal behavior of magnetically marked solid dosage forms," *Advanced drug delivery reviews*, vol. 57, no. 8, pp. 1210–1222, 2005.
- [28] C. Kang, L. Fan, Q. Zheng, X. Kang, J. Zhou, and X. Zhang, "Experimental study on the localization of moving object by total geomagnetic field," *Journal of Sensors*, vol. 2017, 2017.
- [29] A. J. Petruska, J. Edelman, and B. J. Nelson, "Model-based calibration for magnetic manipulation," *IEEE Transactions on Magnetics*, vol. 53, no. 7, pp. 1–6, 2017.
- [30] A. Meurer, C. P. Smith, M. Paprocki, O. Čertík, S. B. Kirpichev, M. Rocklin, A. Kumar, S. Ivanov, J. K. Moore, S. Singh, T. Rathnayake, S. Vig, B. E. Granger, R. P. Muller, F. Bonazzi, H. Gupta, S. Vats, F. Johansson, F. Pedregosa, M. J. Curry, A. R. Terrel, Š. Roučka, A. Saboo, I. Fernando, S. Kulal, R. Cimrman, and A. Scopatz, "SymPy: symbolic computing in Python," *PeerJ Computer Science*, vol. 3, p. e103, Jan. 2017. [Online]. Available: <https://doi.org/10.7717/peerj-cs.103>
- [31] T. Pylvänäinen, "Automatic and adaptive calibration of 3d field sensors," *Applied Mathematical Modelling*, vol. 32, no. 4, pp. 575–587, 2008.
- [32] T. Ozyagcilar, "Calibrating an ecompass in the presence of hard and soft-iron interference," *Freescale Semiconductor Ltd*, pp. 1–17, 2012.
- [33] F. Devernay, "C/C++ minpack," <http://devernay.free.fr/hacks/cminpack/>, 2007.
- [34] "Stata," College Station, TX, 2017. [Online]. Available: www.stata.com
- [35] Y. Higuchi, T. Nara, and S. Ando, "Complete set of partial differential equations for direct localization of a magnetic dipole," *IEEE Transactions on Magnetics*, vol. 52, no. 5, pp. 1–10, 2016.
- [36] S. Song, C. Hu, M. Li, W. Yang, and M. Q.-H. Meng, "Real time algorithm for magnet's localization in capsule endoscope," in *2009 IEEE International Conference on Automation and Logistics*. IEEE, 2009, pp. 2030–2035.
- [37] —, "Two-magnet-based 6d-localization and orientation for wireless capsule endoscope," in *2009 IEEE International Conference on Robotics and Biomimetics (ROBIO)*. IEEE, 2009, pp. 2338–2343.
- [38] C. Hu, M. Q.-H. Meng, and M. Mandal, "Efficient magnetic localization and orientation technique for capsule endoscopy," *International Journal of Information Acquisition*, vol. 2, no. 01, pp. 23–36, 2005.
- [39] S. Yabukami, H. Kikuchi, M. Yamaguchi, K. Arai, K. Takahashi, A. Itagaki, and N. Wako, "Motion capture system of magnetic markers using three-axial magnetic field sensor," *IEEE transactions on magnetics*, vol. 36, no. 5, pp. 3646–3648, 2000.
- [40] R. Guignet, G. Bergonzelli, V. Schlageter, M. Turini, and P. Kucera, "Magnet tracking: a new tool for in vivo studies of the rat gastrointestinal motility," *Neurogastroenterology & Motility*, vol. 18, no. 6, pp. 472–478, 2006.
- [41] V. Schlageter, P. Drljaca, R. S. Popovic, and P. KuČERA, "A magnetic tracking system based on highly sensitive integrated hall sensors," *JSME International Journal Series C Mechanical Systems, Machine Elements and Manufacturing*, vol. 45, no. 4, pp. 967–973, 2002.
- [42] J. Lu, Z. Yang, K. Z. Okkelberg, and M. Ghovanloo, "Joint magnetic calibration and localization based on expectation maximization for tongue tracking," *IEEE Transactions on Biomedical Engineering*, vol. 65, no. 1, pp. 52–63, 2018.
- [43] D. Pham and S. M. Aziz, "A real-time localization system for an endoscopic capsule using magnetic sensors," *Sensors*, vol. 14, no. 11, pp. 20910–20929, 2014.
- [44] C. Cheng, X. Huo, and M. Ghovanloo, "Towards a magnetic localization system for 3-d tracking of tongue movements in speech-language therapy," in *2009 Annual International Conference of the IEEE Engineering in Medicine and Biology Society*. IEEE, 2009, pp. 563–566.
- [45] S. Su, W. Yang, H. Dai, X. Xia, M. Lin, B. Sun, and C. Hu, "Investigation of the relationship between tracking accuracy and tracking distance of a novel magnetic tracking system," *IEEE Sensors Journal*, vol. 17, no. 15, pp. 4928–4937, 2017.
- [46] J. J. Moré, B. S. Garbow, and K. E. Hillstom, "User guide for MINPACK-1," Argonne National Laboratory Applied Mathematics Division, Argonne, IL, Tech. Rep. ANL-80-74, 1980. [Online]. Available: <https://www.mcs.anl.gov/~more/ANL8074b.pdf>
- [47] A. J. Petruska and J. J. Abbott, "Optimal permanent-magnet geometries for dipole field approximation," *IEEE transactions on magnetics*, vol. 49, no. 2, pp. 811–819, 2013.
- [48] S. Song, X. Qiu, W. Liu, and M. Q.-H. Meng, "An improved 6-d pose detection method based on opposing-magnet pair system and constraint multiple magnets tracking algorithm," *IEEE Sensors Journal*, vol. 17, no. 20, pp. 6752–6759, 2017.
- [49] C. Di Natali, M. Beccani, N. Simaan, and P. Valdastrì, "Jacobian-based iterative method for magnetic localization in robotic capsule endoscopy," *IEEE Transactions on Robotics*, vol. 32, no. 2, pp. 327–338, 2016.
- [50] D. Son, X. Dong, and M. Sitti, "A simultaneous calibration method for magnetic robot localization and actuation systems," *IEEE Transactions on Robotics*, vol. 35, no. 2, pp. 343–352, 2018.



Cameron R. Taylor received the B.S. degree in electrical engineering from Brigham Young University, Provo, UT, USA, in 2014 and the M.S. degree in media arts and sciences from the Massachusetts Institute of Technology (MIT), Cambridge, MA, USA, in 2016. He is currently pursuing the Ph.D. degree in media arts and sciences at MIT. His research interests include electromagnetics, algorithm development, and neural interfacing.



Haley G. Abramson attended the Massachusetts Institute of Technology, Cambridge, MA, USA (B.S. '19). At MIT, she studied computer science and molecular biology. She will pursue the Ph.D. in biomedical engineering from Johns Hopkins University, Baltimore, MD, USA beginning in the fall of 2019. Her research interests include biomechanics and surgical device design.



Hugh M. Herr received the B.A. degree in physics from Millersville University of Pennsylvania, Millersville, PA, USA, in 1990, the M.S. degree in mechanical engineering from the Massachusetts Institute of Technology (MIT), Cambridge, MA, USA, in 1993, and the Ph.D. degree in biophysics from Harvard University, Cambridge, MA, USA, in 1988.

He is a Professor within MIT's Program of Media Arts and Sciences, and codirects MIT's Center for Extreme Bionics. His main research interests include applying principles of limb neuromechanics to the design of wearable robotics for human augmentation and rehabilitation. In the area of human augmentation, he has built elastic shoes and powered leg exoskeletons for walking and running that decrease metabolic demand. In the area of assistive technology, he has developed powered orthotic and prosthetic mechanisms for use as assistive interventions in the treatment of leg disabilities caused by amputation, stroke, cerebral palsy, and multiple sclerosis. He is the author and coauthor of more than 150 peer-reviewed manuscripts and patents within the emerging field of biomechatronics.